Bioorganic Chemistry 91 (2019) 103106

Contents lists available at ScienceDirect

Bioorganic Chemistry

journal homepage: www.elsevier.com/locate/bioorg

Bioactivatable reductive cleavage of azobenzene for controlling functional dumbbell oligodeoxynucleotides

Huajun Lei[b], Mengwu Mo[a], Yujian He[a,d], Ya Wu[c,*], Wufu Zhu[b,*], Li Wu[a,d,*]

[a] School of Chemical Sciences, University of Chinese Academy of Sciences, Beijing 101408, China
[b] Department School of Pharmacy Institution, Jiangxi Science & Technology Normal University, Jiangxi 330013, China
[c] College of Chemistry and Chemical Engineering, Xi'an Shiyou University, Shanxi 710065, China
[d] State Key Laboratory of Natural and Biomimetic Drugs, Peking University, Beijing 100191, China

ARTICLE INFO

Keywords:
Azobenzene
Reductive cleavage
Glutathione
Dumbbell asODNs
Activatable

ABSTRACT

Application of stimuli-responsive bioactive molecules is an attractive strategy due to use for target special tissues and cells. Here, we reported synthesis of an azo-linker, 2,2′-dimethoxyl-4,4′-dihydroxymethylazobenzene (**mAzo**), which was more effectively recognized and cleaved by reducing glutathione (GSH) via comparing with 4,4′-dihydroxymethylazobenzene (**Azo**). In addition, **mAzo** is further exploited to engineer dumbbell asODNs, which could result in the release of asODNs and thus modulate their hybridization to target nucleic acids. The present study is the first example to disclose efficient reductive cleavage of azobenzene by GSH to generate aromatic amine. This would provide a valuable strategy for tunable cell-specific release of ODNs and modulation of known disease-causing gene expression in cancer cells.

1. Introduction

Artificial control of biofunction is one of the currently important and attractive themes for post-genome era, because of its potential application to gene therapy, biotechnology, and nanotechnology. In numerous systems, this is achieved through application of external stimuli such as pH [1–3], temperature [4,5], electric field [6,7] and light [8,9]. Especially, Biological stimuli, endogenously produced in specific cell types, present an attractive alternative to meet this goal due to their high selectivity, substrate specificity and mild operating conditions. Therefore, potential manipulation on the gene in different cells or tissues through regulation of endogenous biological substances will arrest more and more attentions.

In this strategy, an azobenzene linkage is introduced, as an artificial active site, which can be used as a powerful tool for studying living systems. Currently, numerous azobenzene derivatives have usually served as a useful core in several photochemical studies, and those switches are used to control conformational changes in oligonucleotides [10–13], as well as functional outcomes [14–16]. However, certain sides effects on tissues and cells of using UV light *in vivo* have limited the application of such light-responsive molecules in biological systems. Therefore, numerous efforts are devoted to prepare azobenzene compounds, that operated with longer wavelengths of light or resistant to the reducing intracellular environment, enabling photocontrol of molecular processes in intracellular environments [17–20].

Additionally, there were studies to show that azo bond could be scissored by azoreductase/NADPH, produced by the microbial flora present in the colon of the human intestine [21,22], or present in the cytoplasm of hepatic cancer cells [23,24], which is being used in the treatment of colon diseases or liver cancers. Additionally, sodium dithionite as a reducing reagent for azo bond, have been used to create a useful molecular device in fluorescent probes [25,26], therapeutic reagent [27,28] and nanocarrier fields [29,30]. Reductive cleavage of azo bond by hydrazine can be applied in polymer assemblies spheres [31]. However, few studies have reported the use of biological stimuli such as GSH to release active molecules in oligodeoxynucleotides, broadening applicability of these functional residues *in vivo* applications.

We previously reported an effective azobenzene photoswitch, 4,4′-dihydroxymethylazobenzene (**Azo**), which can stabilize the hairpin structure [12,13]. Hence, to preserve the conformational stability of ODNs associated with this unit, we utilize **Azo** as a nucleus to develop azobenzene linkers. A comparative investigation of GSH-induced reduction of **Azo** and its derivative, **mAzo**, was performed by UV–Vis spectra, fluorescence spectroscopy, and HPLC analysis. Furthermore, the azobenzene linkers were inserted between 18-mer asODNs and different short protective strands, forming a series of activatable dumbbell oligodeoxynucleotides. The reductive cleavage of azobenzene by GSH could result in the release of ODNs and thus modulate the

* Corresponding authors at: School of Chemical Sciences, University of Chinese Academy of Sciences, Beijing 101408, China (L. Wu).
E-mail addresses: wuya@xsyu.edu.cn (Y. Wu), zhuwf@jxstnu.edu.cn (W. Zhu), wuli@ucas.ac.cn (L. Wu).

https://doi.org/10.1016/j.bioorg.2019.103106
Received 4 March 2019; Received in revised form 2 July 2019; Accepted 2 July 2019
Available online 03 July 2019

hybridization of asODNs to target DNA molecules. These findings would be valuable for further developing GSH-responsive DNA-based molecular devices as treatments for cancer and other diseases in human clinical trials.

2. Results and discussion

2.1. Design and synthesis of azobenzene derivatives and azobenzene linked dumbbell asODNs

In recent photochemical studies of azobenzene conjugates, much effort focuses on how to resist to reduction by GSH [17–20], resulting in more adaptation to intracellular environment. On the other hand, these aromatic azo-linkers are engineered to be effectively cleaved by biological stimuli, releasing the loaded functional molecules selectively [25,27,30,32–35], which can be used for site specific drug delivery [21,22,36,37] and polymer self-assembly [38–40]. Earlier reports showed that incorporating the electron-rich substituents of aromatic azobenzene will increase their susceptibility to cleavage by azoreductase enzymes [24]. When the electron-donating oxygen (O) or nitrogen (N) groups in the para and ortho positions were incorporated into the aromatic azobenzene ring, the cleavage level of azobenzene bond was improved.

In this work, **Azo** has served as a useful core in which two terminal hydroxymethyl groups as reactive group were able to covalently attach to oligodeoxynucleotides. In order to identify the sensitivity of azobenzene analogues with GSH, di-electron-donating oxygen ($-OCH_3$) groups in the ortho positions of azobenzene were incorporated to control the electronegativity of azobenzene derivatives and enhance their cleavage rates by reduction agents.

To test effective cleavage of **mAzo** in system with oligodeoxynucleotides, the azobenzene unit is inserted between 18-mer asODNs and 4, 5 and 6 short protective strands, respectively. Similar to our previous report [13], a series of azobenzene linked dumbbell asODNs were formed, and the antisense ODN strands were temporally sequestered. In the presence of GSH, azo bonds were cleaved to respective aromatic amine, and two terminal protective strands of ODN hairpins were easily detachable, resulting in release of the asODNs, allowing asODN fragments to hybridize their complementary target DNA (Scheme 1).

mAzo was synthesized from methyl 4-amino-3-methoxybenzoate, with pyridine as a ligand and CuBr as the catalyst following published protocols [41] (Fig. S1, ESI[†]). As control, synthesis of **Azo** referred to our previous report [13]. To incorporate the azo-linker in dumbbell asODNs, one alcohol group of two aromatic rings was protected by DMT group, and the other one followed by reaction with N,N,N′,N′-tetraisopropyl-phosphorodiamidite (Fig. S1, ESI[†]), which formed an analogue of DNA phosphoramidites to couple with general DNA monomers by solid-phase synthesis method. Thus, a series of azobenzene linked dumbbell asODNs were formed and shown in Fig. 1. The dumbbell asODNs were designated to be **AZ18O-4**, **AZ18O-5** and **AZ18O-6** for **mAzo**-linked 18-mer asODNs with 4–6 nt hairpin stems, and **AZ18P-4**, **AZ18P-5** and **AZ18P-6** for **Azo**-linked 18-mer asODNs with 4–6 nt hairpin stems, respectively.

2.2. Reductive cleavage of azobenzene derivatives by GSH

A comparative investigation of GSH-induced of **Azo** and its derivative, 2,2′-dimethoxyl-4,4′-dihydroxymethylazobenze-ne (**mAzo**), is performed by UV–Vis spectra, fluorescence spectroscopy and HPLC analysis. It is reported that the content of GSH in cancer cells is 10–14 mM [42,43]. To make it easier to observe the high cleavage efficiency for mAzo with methoxy groups at the ortho-position, the concentration of GSH was increased to cleave the azo compounds *in vitro* study. **mAzo** and **Azo** were incubated with 25 mM GSH in PBS buffer (0.1 M, pH 7.0) containing 2 μL DMSO at 37 °C for different times

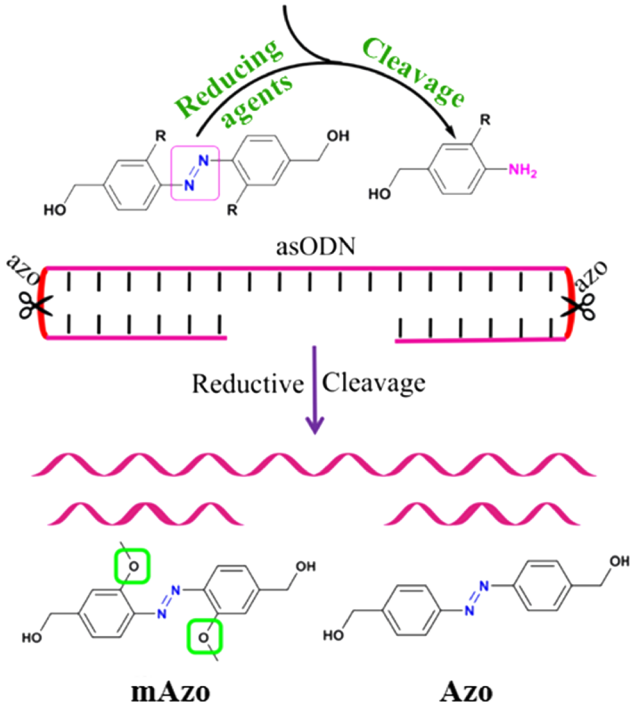

Scheme 1. Schematic illustration of reductive cleavage of azobenzene derivates by glutathione and release of asODNs from activatable dumbbell oligodeoxynucleotides.

AZ18P-4	5'-GGAG**azo**CTCCTCGCCCTTGCTCAC**azo**GTGA-3'
AZ18P-5	5'-AGGAG**azo**CTCCTCGCCCTTGCTCAC**azo**GTGAG-3'
AZ18P-6	5'-GAGGAG**azo**CTCCTCGCCCTTGCTCAC**azo**GTGAGC-3'
AZ18O-4	5'-GGAG**mAzo**CTCCTCGCCCTTGCTCAC**mAzo**GTGA-3'
AZ18O-5	5'-AGGAG**mAzo**CTCCTCGCCCTTGCTCAC**mAzo**GTGAG-3'
AZ18O-6	5'-GAGGAG**mAzo**CTCCTCGCCCTTGCTCAC**mAzo**GTGAGC-3'
MB-7	5'- GCGTACGGTGAGCAAGGGCGAGGAGCGTACGC-3'
AZ18	5'-CTCCTCGCCCTTGCTCAC-3'
AZ23	5'- AGGAGCTCCTCGCCCTTGCTCAC-3'

Fig. 1. Sequences of azobenzene linked dumbbell asODNs, control ODNs (**AZ18** and **AZ23**), and target DNA (**MB-7**) used in this study.

(0 h, 3 h, 6 h, 12 h, 18 h and 24 h). The results showed that UV absorbance of **mAzo** at 370 nm (λ_{max} for **mAzo**) obviously decreased upon incubation with GSH for 3 h, and reached a plateau within 24 h, accompanying with color change of the reaction solution from golden to white (Fig. S2, ESI[†]). This indicated that the **mAzo**-linker was effectively reduced by GSH and the azo bond chromophore was removed from the molecular structure (Fig. 2A). In contrast, UV absorbance of **Azo** at around 340 nm (λ_{max} for **Azo**) remained almost constant upon incubation with GSH for 24 h under the same conditions (Fig. 2B). In addition, the reaction processes of reductive cleavage for **mAzo** and **Azo** were monitoring by fluorescence emission spectra. Similarly, fluorescence intensity of reaction mixture of **mAzo** displayed a remarkable increase at 420 nm (λ_{em} for **mAzo**) when incubated with GSH for 24 h, where as fluorescence intensity at 440 nm (λ_{em} for **Azo**) of reaction system for **Azo** still kept at a constant value (Fig. 2C and 2D). Moreover, a characteristic band of N—H wagging vibration at 900–650 cm^{-1} for cleavage product was increased using FT-IR spectra when compared with the raw **mAzo** (Fig. S3, ESI[†]), which further confirms **mAzo** was reductively cleaved to aromatic amine.

The reductive cleavage of **mAzo** and **Azo** in response to GSH was further assessed by HPLC analysis. As shown in Fig. 3A, the peaks at 8.7 min and 7.9 min are identified as trans form and cis form of **mAzo**, respectively. Upon incubation of **mAzo** with GSH for 3 h, the new main peak appeared at 6.3 min and increasing incubation time caused a concomitant increase in the amount of main product, which followed a similar trend to that observed by UV and fluorescence analysis. The ESI-

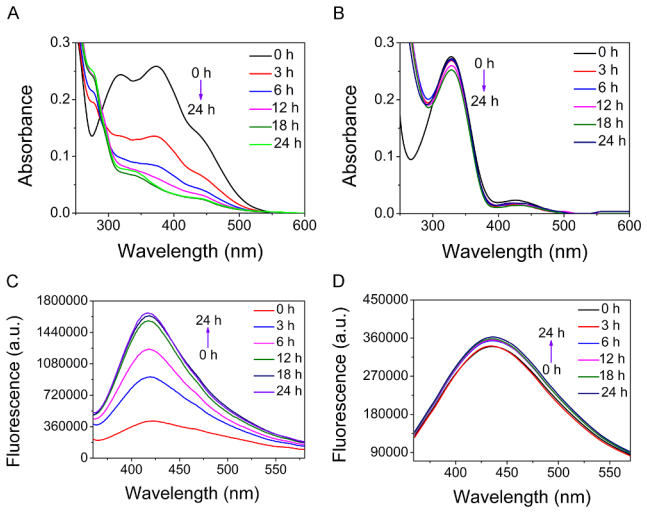

Fig. 2. UV–Vis absorbance spectra and fluorescence spectra of **mAzo** and **Azo** upon incubation with GSH. The absorbance changes for **mAzo** (A) and **Azo** (B) and fluorescence changes for **mAzo** (C) and **Azo** (D) were recorded when incubated with GSH (25 mM) at 37 °C for 0 h, 3 h, 6 h, 12 h, 18 h and 24 h in PBS buffer (0.1 M, pH 7.0) containing 2 μL DMSO.

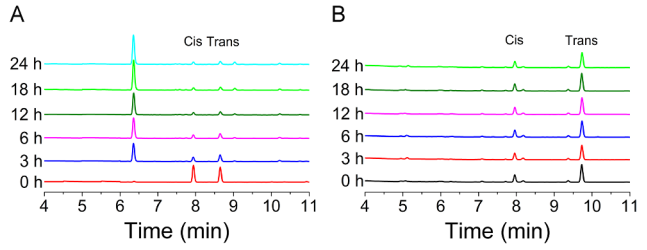

Fig. 3. HPLC analysis of the GSH-mediated cleavage reactions for **mAzo** (A) and **Azo** (B). HPLC results were recorded when GSH (25 mM) was added and incubated at 37 °C for 0 h, 3 h, 6 h, 12 h, 18 h and 24 h.

MS (Fig. S4, ESI†) and GC–MS (Fig. S5, ESI†) analysis for the main cleaved product showed 4-amino-3-methoxyphenylmethanol was produced by azo bond cleavage. Differently, no new peak was observed for **Azo** incubated with GSH for 24 h (Fig. 3B).

To probe the cleavage level of azobenzene compounds in mimic cancer cell conditions, the degradation studies of **mAzo** and **Azo** were carried out in the presence of 10 mM reduced glutathione. We simultaneously used UV–Vis spectra and HPLC to monitor the azo bond cleavage in solution upon incubation of **mAzo** or **Azo** with GSH. Result revealed that incubation of **mAzo** with GSH has similar variation trend in the presence of 10 mM GSH (Fig. S6A and S6C, ESI†), although low concentration of GSH (10 mM) reacted with **mAzo** was less completely than high concentration of GSH (25 mM). By contrast, we could not detect the cleavage of **Azo** under the same conditions (Fig. S6B and S6D, ESI†). The observed results clearly showed that GSH indeed triggered the reductive cleavage for **mAzo** but not for **Azo** under the same conditions, which correlates with incorporation of electron-donating groups (–OCH_3) in the ortho position.

2.3. Mechanistic study

Prompted by the observation that proteinogenic thiols reduce azobenzene [44], we incubated **mAzo** with cysteine containing thiol as a positive control. Results showed that a reduction in UV absorbance was reduced (Fig. S7, ESI†), indicating that **mAzo** can be reduced by cysteine. HPLC analysis simultaneously showed that a new peak appeared

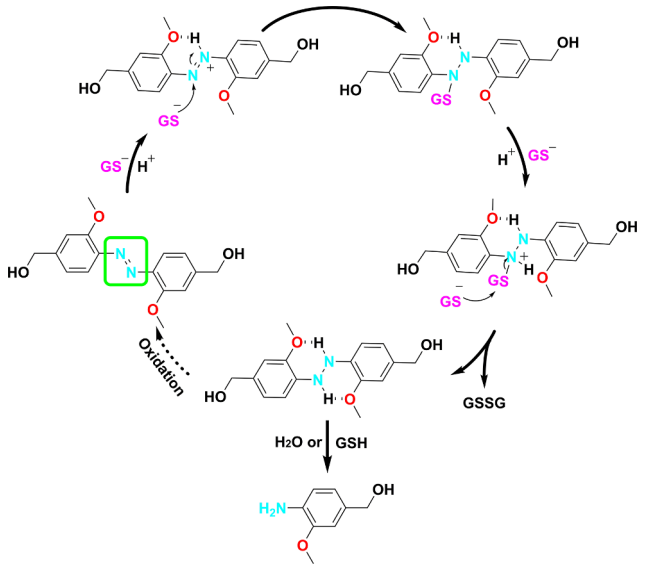

Fig. 4. Proposed the reaction mechanism of **mAzo** with GSH.

at 6.3 min (Fig. S8, ESI†), corresponding to 4-amino-3-methoxyphenylmethanol. Comparing with cysteine, alanine without thiol did not induce change in UV absorbance of **mAzo**. Those results collectively showed that the azo bond of **mAzo** was digested by thiol, which agreed with the mechanism of reduction by thiol for diazenedicarboxylic acid derivatives, presented initially by Kosower [45]. This process involved that the thiol attacked one azo nitrogen atom, and the second azo nitrogen atom became protonated to give a sulfenyl hydrazine derivative. However, **mAzo** was more electron rich in ortho substituted position, and thus protonation of the azo group occurred by prior, or concomitant, giving six-membered intermediate, due to the formation of H-bonding to the methoxyl group in the planar conformation (Fig. 4). In the present case, thiol attack is facilitated by increasing the electrophilicity of the diazo system. This leads to an unstable sulfenyl hydrazine intermediate, which is further reattached by a proton with the assistance of GS^-, producing an unstable hydrazo intermediates. It is easily reduced cleaving the N—N bond into its respective amines with addition of H_2O or GSH. Combined with the GSH and Cys results, we observed that the degree of reaction of **mAzo** with GSH was more completely than Cys, which would be attributed to the relatively low pH value of GSH reaction system, due to GSH has two carboxyl groups.

Additionally, effect of the isomers of **mAzo** on GSH-induced reducing cleavage was assessed. The parallel **mAzo** solutions were added with GSH, irradiated respectively with UV (365 nm, 7 mW/cm^2) and visible light (> 400 nm, 11 W) for 5 min at room temperature, and then incubated under same conditions for various times, respectively. The HPLC data showed that **mAzo** mostly took a cis configuration upon UV irradiation where as it exists dominantly in the cis form with visible light irradiation at room temperature. This finding was explained by the slight difference between these two energy states in water according to the results of energy calculations of trans-**mAzo** and cis-**mAzo** in water and methanol (Figs. S9 and S10, ESI†). Furthermore, for two reaction systems of **mAzo** upon UV irradiation and visible light irradiation, the spectral changes displayed that UV absorbance at 370 nm gradually decreased after incubating with GSH until it reached a constant value after 24 h incubation (Fig. S11, ESI†), indicating both isomers of the **mAzo** were reduced by GSH. HPLC analysis displayed their reduction by GSH, which produced the amine product (Fig. S12, ESI†). What's more, GSH-induced reaction with cis-mAzo has relatively higher reaction rate than trans-mAzo by quantitative analysis of cleaved products of **mAzo** after UV irradiation and visible light irradiation (Fig. S13, ESI†).

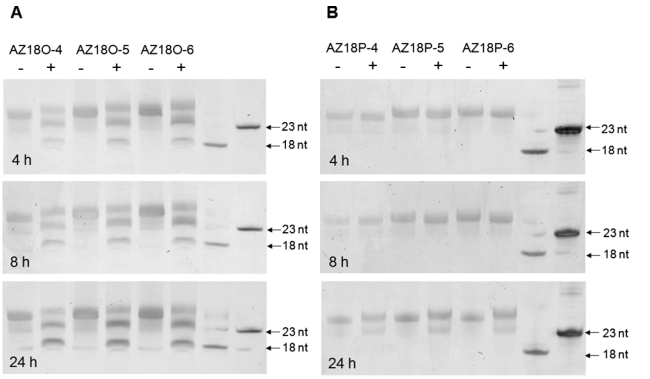

Fig. 5. 20% denaturing PAGE of cleavages of **mAzo** (A) and **Azo** (B) linked dumbbell asODNs with incubating 25 mM GSH at 37 °C for 4 h, 8 h and 24 h. "−" and "+" correspond to the dumbbell asODN without and with GSH, respectively.

2.4. GSH-induced azobenzene cleavage for application in dumbbell asODNs

AsODNs have been proven effective in gene silencing in many experimental systems and are being developed as treatments for cancer and other diseases in human clinical trials [46]. For the regulation of gene expression, an antisense strategy based on the hybridization of target mRNA with antisense DNA has been widely adopted. As expected, based on our previous work with azobenzene linked dumbbell asODNs [13], the dumbbell asODNs effectively controlled the DNA/RNA or DNA/DNA hybridization to regulate target RNA digestion through azobenzene photoisomerization. Since GSH is more widely existed in cancer cells than normal cells [5,47,48], we will seek to develop GSH-induced release of asODNs for modulating the hybridization of asODNs to target DNA or RNA molecules.

To confirm that reductive cleavage of azobenzene and release of asODNs are selectively triggered by GSH, the **mAzo** conjugates and **Azo** conjugates were incubated with GSH at 37 °C for 4 h, 8 h and 24 h while monitoring release of asODNs by denaturing polyacrylamide gel electrophoresis (PAGE). Fig. 5 showed results of reducing cleavage of these dumbbell asODNs in absence or presence of GSH. Lanes 1, 3, 5 and lanes 2, 4, 6 in each panel showed the mobility of the dumbbell asODNs without and with GSH, respectively. Obviously, cleavage of **mAzo** linked dumbbell asODNs (**AZ18O-4**, **AZ18O-5** and **AZ18O-6**) occured upon incubation with GSH for 4 h and the major bands were the cleavage products of one **mAzo**-linker. With increasing incubation time, two **mAzo**-linkers were gradually cleaved and caused a significant increase of 18-mer asODNs after 24 h incubation (Fig. 5A). However, for **Azo** linked dumbbell asODNs (**AZ18P-4**, **AZ18P-5** and **AZ18P-6**), there was no obvious increase of cleaved bands within 8 h under the same GSH assay conditions and even no product bands of 18-mer asODNs after 24 h (Fig. 5B). This clearly shows that GSH reduction of the **mAzo**-linker is the "trigger" responsible for asODN release. By quantifying the percentage of cleaved dumbbell asODNs after incubating for 24 h, 87.8%, 88.0% and 88.9% of **mAzo** linkers were cleaved for **AZ18O-4**, **AZ18O-5** and **AZ18O-6** by GSH, while only 24.4%, 23.8% and 20.3% dumbbell asODNs were reductively cleaved for **AZ18P-4**, **AZ18P-5** and **AZ18P-6**. This indicated that the cleavage efficiencies were almost independent of numbers of binding arms for the dumbbell asODNs.

To further confirm GSH-induced binding target DNA with azobenzene linked dumbbell asODNs, based on many biological activities of asODNs involving the hybridization, GSH-induced release of asODN for modulating the hybridization between asODN and target DNA or RNA was investigated using native PAGE. Different from existed form of stable isomers of only **mAzo**, **mAzo** in dumbbell asODNs displayed the main conformation in trans state without irradiation, according to the photoisomerization of **mAzo** linked dumbbell asODNs with UV and visible light irradiation (Fig. S14, ESI[1]). The results of these dumbbell asODNs binding to target DNA (**MB-7**) in absence or presence of GSH at 37 °C were shown in Fig. 6. With this system, these asODNs with dumbbell structures should lead to binding competition to asODN fragments between two binding arms and their target DNA. As the number of binding arms increased for the dumbbell ODNs (**AZ18O-4**, **AZ18O-5** and **AZ18O-6**), the binding ability between dumbbell asODN and target DNA (**MB-7**) was weakened (Fig. 6A, Lanes 2, 4 and 6). Indeed, Fig. 6A showed **AZ18O-6** (2.0%) with two longer binding arms produced much lower "background" binding than **AZ18O-4** with two shorter binding arms (54.3%).

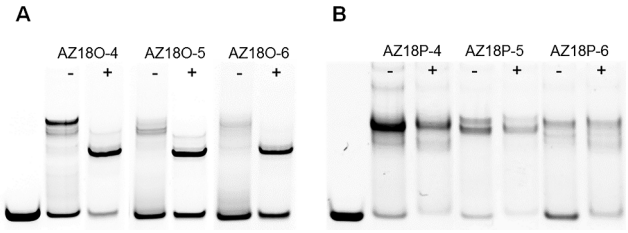

Fig. 6. 20% Native PAGE of the binding of **mAzo** (A) and **Azo** (B) linked dumbbell asODNs (2 μM) with **MB-7** (2 μM) in 1 × PBS buffer at 37 °C after 24 h incubation. Lane 1: **MB-7**. "−" and "+" correspond to the dumbbell asODN and **MB-7** without and with GSH, respectively.

In addition, as shown in **mAzo**-linker's reduction (Fig. 3A) and the associated ODN release profile (Fig. 5A), the total amount of binding products of **AZ18O-4**, **AZ18O-5** and **AZ18O-6** with **MB-7** showed slight differences upon incubation of the dumbbell ODNs with GSH (Fig. 6A, Lanes 3, 5 and 7). However, incubation of the dumbbell ODNs with GSH for 24 h can distinctly distinguish the difference in binding of the dumbbell ODNs to **MB-7**. For example, the incubation with GSH caused an increase in binding products of **AZ18O-4**, **AZ18O-5** and **AZ18O-6** from 54.3%, 14.2% and 2% to 80.5%, 67.6%, and 57.6%, which were about 1.5, 4.8 and 28.8-fold increase, respectively (Fig. 6A). Specifically, of the different dumbbell ODNs studied, **AZ18O-6** with 6 nt nucleobases in binding arms was by far most efficient for binding to target DNA. This indicated that the GSH-induced dumbbell ODNs for binding to target gene depended on not only azobenzene linker but also the length of protective strand of the dumbbell ODNs. Compared with regulation of the target DNA using the dumbbell asODNs upon light irradiation [13], GSH-mediated activation of the dumbbell asODNs showed much higher efficiency. For **Azo** system, with the numbers of binding arms increased, binding ability of dumbbell asODNs and target **MB-7** followed a same trend as **mAzo** system in the absence of GSH (Fig. 6B, Lanes 2, 4 and 6). On the other hand, no much stronger hybridization bands were observed for **AZ18P-4**, **AZ18P-5** and **AZ18P-6** with GSH reduction, which indicates that all of the **Azo** modified asODNs were less sensitive to GSH.

3. Conclusions

In summary, 2,2′-dimethoxyl-4,4′dihydroxymethyl (**mAzo**) described here can be more effectively cleaved by reductive glutathione. Furthermore, an "intelligent" azobenzene-conjugate system with oligodeoxynucleotides was engineered to yield asODNs to bind target DNA with respond to GSH. Taken together, the current research on the orthomethoxyl substituted azobenzene derivatives provided a novel strategy on GSH-induced molecular responses, and its attachment to a wide variety of targets can be extended versatility of azobenzene for *in vivo* use. Interestingly, intracellar GSH concentration is much higher in cancer cells than normal cells. The reductive cleavage of azobenzene will be important for controlling cancer gene and developing prodrug.

4. Experimental

4.1. Chemicals and techniques

All the reagents for organic synthesis were analytically pure and solvents for synthesis and purification were distilled over CaH_2. All oligonucleotides were custom-synthesized on ABI 394 DNA/RNA synthesizer (Applied Biosystems). Deprotected oligonucleotides were purified with an Agilent 1260 system using Agilent reverse phase C18 column (5 μm bead, 9.6 mm × 150 mm). The UV–Vis spectra were measured on a Shimadzu UV-1800 model spectrophotometer. All fluorescence spectra were recorded in JOBIN YVON Fluoromax-4. Analytical PAGE was carried out on BioRad ChemiDoc™ MP Imaging System. UV irradiation *in vitro* experiments were carried out using UV-LED lamp (365 nm, 7 mW/cm^2). Visible irradiation was performed using general energy-efficient lamp (> 400 nm, 11 W). ^{1}H NMR and ^{13}C NMR spectra were recorded using JNM-ECZ400S (400 MHz for ^{1}H, 100 MHz for ^{13}C). Mass spectra were obtained using GC–MS and ESI-MS.

4.2. Synthesis

4.2.1. Synthesis of compound **1**

CuBr (14.3 mg, 0.1 mmol), pyridine (23.7 mg, 0.3 mmol), and methyl 4-amino-3-methoxybenzoate (362 mg, 2.0 mmol) were mixed in toluene (20 mL) under an O_2 atmosphere (1 atm). The reaction mixture was vigorously stirred at 60 °C for 24 h. After cooling down to room temperature and concentrating under vacuum, the crude product was purified by column chromatography on silica gel using petroleum ether and ethyl acetate (V/V = 8:1) as eluents, to afford 89.5 mg (in yield 25%) of dimethyl 4,4′-(diazene-1,2-diyl)-bis(3-methoxybenzoate) as a red solid. ^{1}H NMR ($CDCl_3$, 400 MHz) δ 7.76 (d, J = 1.4 Hz, 1H), 7.68 (dd, J = 1.2 Hz, 8.0 Hz, 1H), 7.62 (d, J = 8.4 Hz, 1H), 4.08 (s, 3H), 3.95 (s, 3H). ^{13}C NMR ($CDCl_3$, 100 MHz) δ 166.51, 156.66, 145.38, 133.57, 122.27, 117.55, 113.64, 56.55, 52.61.

4.2.2. Synthesis of compound **2**

300 mg (0.84 mmol) of intermediate (dimethyl 4,4′-(diazene-1,2-diyl)-bis(3-methoxybenzoate)) was dissolved in 20 mL dry THF, then 95.63 mg (2.52 mmol) of $LiAlH_4$ was slowly added into solution while stirring vigorously for 6 h at room temperature, and reaction was quenched by 5 mL of 95% ethanol. Then, the precipitate was filtered and washed with ethanol. Finally, the filtrate was concentrated by rotary evaporation to obtain a yellow solid. The crude product was purified by silica gel chromatography with petroleum ether/ethyl acetate (volume ratio: 2/1) to give orange solids (228.5 mg) in yield 90%. ^{1}H NMR (CD_3OD, 400 MHz) δ 7.57 (d, J = 8 Hz, 1H), 7.22 (s, 1H), 6.99 (d, J = 8 Hz, 1H), 4.67 (s, 2H), 4.02 (s, 3H). ^{13}C NMR (CD_3OD, 100 MHz) δ 158.40, 148.07, 142.95, 119.84, 118.05, 112.07, 64.81, 56.72.

4.2.3. Synthesis of compound **3**

mAzo (300 mg, 1.0 mmol) was dissolved in anhydrous THF (5 mL), and Triethylamine (TEA, 100 μL) was added to the solution and then 4,4′-dimethoxytrityl chloride (DMT-Cl, 169 mg, 0.5 mmol) was added to the mixture, which was stirred for 3 h at 60 °C. After monitoring the reaction progress by thin-layer chromatography (TLC), DMT-Cl (119 mg, 0.35 mmol) was added, and the solution stirred for an additional 2 h at 60 °C. After the reaction was completed, all solvents were evaporated under reduced pressure. The crude product was purified by silica gel column chromatography (petroleum ether/ethyl acetate/Triethylamine = 25/10/1) to obtain compound **3** as a red solid (242 mg) in yield 80%. ^{1}H NMR ($CDCl_3$, 400 MHz) δ 7.64 (d, J = 4 Hz, 1H), 7.62 (d, J = 4 Hz, 1H), 7.52 (d, J = 8 Hz, 2H), 7.42 (d, J = 4 Hz, 2H), 7.40 (d, J = 2 Hz, 2H), 7.31(t, J = 7.6 Hz, 2H), 7.22 (d, J = 7.2 Hz, 1H), 7.11 (d, J = 5.6 Hz, 2H), 7.01 (d, J = 8.4 Hz, 1H), 6.95 (d, J = 8.4 Hz, 1H), 6.87 (s, 2H), 6.84 (s, 2H), 4.75 (s, 2H), 4.24 (s, 2H), 4.02 (d, J = 3.2, 6H), 3.80 (s, 6H). ^{13}C NMR ($CDCl_3$, 100 MHz) δ 158.59, 157.05, 156.91, 145.01, 144.32, 142.21, 141.86, 136.20, 130.14, 128.22, 128.03, 126.96, 119.12, 118.94, 117.61, 117.37, 113.27, 110.79, 110.69, 86.71, 65.53, 65.09, 56.41, 55.34.

4.2.4. Synthesis of azobenzene linked dumbbell asODNs

Compound **3** (300 mg, 0.51 mmol) and 1H-tetrazole (14.3 mg, 0.21 mmol) were dissolved in anhydrous acetonitrile (3.4 mL), and then 2-cyanoethyl-N,N,N,N-tetraisopropylphosphoradiamidite (138.3 mg, 0.46 mmol) was added to the solution. The mixture was stirred under Nitrogen atmosphere, and the reaction was monitored by TLC (yield was estimated above 90%). After one hour later, the solution was filtered using hydrophobic membrane filter and moved to a vial for application to DNA synthesis without further purification. The synthesis process and the structure characterization were shown in Fig. S1. 4,4′-bis(hydroxymethyl)azobenzene phosphoramidite and 4,4′-bis(hydroxymethyl)-3,3′-dimetho-

xyazobenzene phosphoramidite were introduced to the dumbbell ODNs by facile synthetic methods of solid phase phosphoramidite chemistry. DNA synthesis was performed using standard phosphoramidite chemistry, and standard procedure for solid-phase oligonucleotide synthesis was used for the synthesis of all oligonucleotides. Standard synthetic cycles provided by Applied Biosystems were used for all normal bases. The azobenzene phosphoramidites without further purification were adjusted to 0.15 M solutions. Coupling time was extended to 30 min for modified nucleotides to maximize the coupling yield. The step coupling efficiencies were close to those of normal deoxynucleotide phosphoramidites.

4.2.5. Purification of azobenzene linked dumbbell asODNs

The oligonucleotides were treated with concentrated ammonium hydroxide for 12 h at 50 °C to cleave them from solid supports and deprotect the phosphates and nucleobases. The solid supports were then filtered out and the filtrates were concentrated to dryness. Oligonucleotide purification was performed by a RP-HPLC with Agilent reverse phase C18 column (5 μm, 9.4 mm × 250 mm) using 0.05 M triethylammonium acetate (TEAA, phase A) and acetonitrile (phase B) as eluents. The samples eluted at 1.0 mL/min with running temperature at 40 °C and a gradient of acetonitrile (B): 0–40% in 40 min, 40–100% in 45 min, 100% in 50 min, 100–10% in 55 min, 10% in 60 min. The objective preparative eluent was collected after the analysis running on HPLC was monitored for UV absorption at 260 nm. All the obtained oligonucleotides were characterized by ESI-MS under negative mode (1 μL sample (100 μM) in H_2O/CH_3CN (1:1) and 1% TEA). The amounts of DNA were determined by UV absorbance at 260 nm using NanoDrop (Thermo scientific).

4.2.6. UV–Vis spectra and HPLC characterization

A stock solution (3.3 mM) of **mAzo** and **Azo** in DMSO was prepared, then added 30 μL GSH (25 mM), 2 μL PBS (0.1 M, pH 7.0), and 4 μL $MgCl_2$ (5 mM) to 600 μL bottle. After completed, the reaction was diluted with ultrapure water to obtain the desired concentration, and the change of absorbance was monitored using an UV1800 Spectrophotometer. At the same time, the same samples were analyzed using a C18 (5 μm, 4.6 × 250 mm) column connected to an Agilent HPLC system equipped with a UV dual absorbance detector. A mixture of water and acetonitrile was used as a mobile phase to separate product and crude material on the C18 column using a H_2O:ACN gradient of 30:90 in 10 min, 10:90 in 11–14 min, and 90:10 in 15–17 min at a flow rate of 1 mL/min. Absorbance of eluting reductive cleavage product molecules was measured at 287 nm.

4.2.7. Polyacrylamide gel electrophoresis (PAGE) characterization

GSH (25 mM) were added to equimolar solutions of azobenzene modified dumbbell ODNs (2 μM) dissolving in PBS buffer (0.1 M, pH = 7.0) and $MgCl_2$ (5 mM), and then respectively incubated for 4 h,

8 h, 24 h at 37 °C while shaking at 210 rpm. Before the samples were loaded into the gel, appropriate 2 × glycerol gel loading buffer containing bromophenol blue was added. All appropriate solutions were loaded into 20% denaturing polyacrylamide gels containing 7 M urea. The gels were then electrophoresed at 150 V for 1.5 h at room temperature, using 1 × TBE buffer Gels were imaged with a BioRad ChemiDoc™ MP Imaging System.

4.2.8. Binding studies

The solutions of the fluorescein labelled **MB-7** (2 μM) with azobenzene modified ODNs (2 μM) and GSH (25 mM) in 4 μL 1 × PBS buffer was used for binding assays. The mixture solution was incubated at 37 °C for 24 h and was then concentrated. Before the samples were loaded into the gel, 1 μL 6 × sucrose gel loading buffer containing bromophenol blue was added. All 6 μL solutions were loaded into 20% native polyacrylamide gels. The gels were then electrophoresed at 150 V for 1.5 h at room temperature, using 1 × TBE buffer. Gels were imaged with a BioRad ChemiDoc™ MP Imaging System.

Supporting information

The supporting information is available online at http://chem.scichina.com and http://link.springer.com/journal/11426. The supporting informations are published as submitted, without typesetting or editing. The responsibility for scientific accuracy and content remains entirely with the authors.

Acknowledgments

This work was supported by National Natural Science Foundation of China (Nos. 21778054, 51772289), Beijing Natural Science Foundation (No. 2192058), National Key Research and Development Plan of China (No. 2016YFF0203703), Fusion Project of Molecular Science and Education for Institute of Chemistry (No. Y82901NED2), UCAS Students' Entrepreneurship Research (No. 118900EA12), Open Project Fund of State Key Laboratory of Natural and Biomimetic Drugs (No. K20150204).

Declaration of Competing Interest

The authors declare that they have no conflict of interest.

Appendix A. Supplementary material

Supplementary data to this article can be found online at https://doi.org/10.1016/j.bioorg.2019.103106.

References

[1] L. Li, Y. Jiang, C. Cui, Y. Yang, P. Zhang, K. Stewart, X. Pan, X. Li, L. Yang, L. Qiu, W. Tan, Modulating aptamer specificity with pH-responsive DNA bonds, J Am Chem Soc 140 (2018) 13335–13339.
[2] P. Li, Z. Chen, Y. Huang, J. Li, F. Xiao, S. Zhai, Z. Wang, X. Zhang, L. Tian, A pH responsive fluorescent probe based on dye modified i-motif nucleic acids, Org Biomol Chem 16 (2018) 9402–9408.
[3] X. Xu, J. Wu, Y. Liu, M. Yu, L. Zhao, X. Zhu, S. Bhasin, Q. Li, E. Ha, P.J. Shi, O.C. Farokhzad, 2016-Ultra pH responsive and tumor penetrating nanoplatform for targeted siRNA delivery with robust anticancer efficacy, Angew Chem Int Ed 55 (2016) 7091–7094.
[4] J.H. Lee, H.A. Ji, Regulation of temperature-responsive flowering by MADS-box transcription factor repressors, Science 342 (2013) 628–632.
[5] S. Mura, J. Nicolas, P. Couvreur, Stimuli-responsive nanocarriers for drug delivery, Nat Mater 12 (2013) 991–1003.
[6] E.A. Hemmig, C. Fitzgerald, C. Maffeo, L. Hecker, S.E. Ochmann, A. Aksimentiev, P. Tinnefeld, U.F. Keyser, Optical voltage sensing using DNA origami, Nano Lett 18 (2018) 1962–1971.
[7] Y. Wei, Q. Zeng, J. Huang, Q. Hu, X. Guo, L. Wang, An electro-responsive imprinted biosensor with switchable affinity toward proteins, Chem Commun 54 (2018) 9163–9166.
[8] Y. Ji, J. Yang, L. Wu, L. Yu, X. Tang, Photochemical regulation of gene expression using caged siRNAs with single terminal vitamin E modification, Angew Chem Int Ed 55 (2016) 2152–2156.
[9] L. Wu, Y. Wang, J. Wu, C. Lv, J. Wang, X. Tang, Caged circular antisense oligonucleotides for photomodulation of RNA digestion and gene expression in cells, Nucleic Acids Res 41 (2013) 677–686.
[10] T.I. Hiroyuki Asanuma, Takayuki Yoshida, Xingguo Liang, Makoto Komiyama, Photoregulation of the formation and dissociation of a DNA duplex by using the cis–trans isomerization of azobenzene, Angew Chem Int Ed 38 (1999) 2393–2395.
[11] T.T. Hiroyuki Asanuma, Takayuki Yoshida, Daisuke Tamaru, Xingguo Liang, Makoto Komiyama, Enantioselective incorporation of azobenzenes into oligodeoxyribonucleotide for effective photoregulation of duplex formation, Angew Chem Int Ed 40 (2001) 2671–2673.
[12] L. Wu, K. Koumoto, N. Sugimoto, Reversible stability switching of a hairpin DNA via a photo-responsive linker unit, Chem Commun (2009) 1915–1917.
[13] L. Wu, Y. Wu, H. Jin, L. Zhang, Y. He, X. Tang, Photoswitching properties of hairpin ODNs with azobenzene derivatives at the loop position, Med Chem Commun 6 (2015) 461–468.
[14] H. Asanuma, X. Liang, H. Nishioka, D. Matsunaga, M. Liu, M. Komiyama, Synthesis of azobenzene-tethered DNA for reversible photo-regulation of DNA functions: hybridization and transcription, Nature Protocols 2 (2007) 203–212.
[15] D. Kong, M. Mo, H. Ji, H. Lei, L. Chen, Y. Li, Y. He, X. Tang, P. Zheng, L. Wu, Reversible photoregulation in biological systems via introduction of azobenzene into nucleic acid, Sci Sin Chim 48 (2018) 698–711.
[16] L. Wu, Y. He, X. Tang, Photoregulating RNA digestion using azobenzene linked dumbbell antisense oligodeoxynucleotides, Bioconjug Chem 26 (2015) 1070–1079.
[17] M. Dong, A. Babalhavaeji, C.V. Collins, K. Jarrah, O. Sadovski, Q. Dai, G.A. Woolley, Near-infrared photoswitching of azobenzenes under physiological conditions, J Am Chem Soc 139 (2017) 13483–13486.
[18] S. Samanta, A. Babalhavaeji, M.X. Dong, G.A. Woolley, Photoswitching of ortho-substituted azonium ions by red light in whole blood, Angew Chem Int Ed 52 (2013) 14127–14130.
[19] S. Samanta, A.A. Beharry, O. Sadovski, T.M. McCormick, A. Babalhavaeji, V. Tropepe, G.A. Woolley, Photoswitching azo compounds in vivo with red light, J Am Chem Soc 135 (2013) 9777–9784.
[20] S. Samanta, T.M. McCormick, S.K. Schmidt, D.S. Seferos, G.A. Woolley, Robust visible light photoswitching with ortho-thiol substituted azobenzenes, Chem Commun 49 (2013) 10314–10316.
[21] S.R. Deka, S. Yadav, M. Mahato, A.K. Sharma, Azobenzene-aminoglycoside: self-assembled smart amphiphilic nanostructures for drug delivery, Colloid Surface B 135 (2015) 150–157.
[22] A. Popat, B.P. Ross, J. Liu, S. Jambhrunkar, F. Kleitz, S.Z. Qiao, Enzyme-responsive controlled release of covalently bound prodrug from functional mesoporous silica nanospheres, Angew Chem Int Ed 124 (2012) 12654–12657.
[23] D. Ma, C. Huang, J. Zheng, W. Zhou, J. Tang, W. Chen, J. Li, R. Yang, An azoreductase-responsive nanoprobe for hypoxia-induced mitophagy imaging, Anal Chem 91 (2019) 1360–1367.
[24] S.H. Medina, M.V. Chevliakov, G. Tiruchinapally, Y.Y. Durmaz, S.P. Kuruvilla, M.E. Elsayed, Enzyme-activated nanoconjugates for tunable release of doxorubicin in hepatic cancer cells, Biomaterials 34 (2013) 4655–4666.
[25] S.S. Liew, S. Du, J. Ge, S. Pan, S.Y. Jang, J.S. Lee, S.Q. Yao, A chemoselective cleavable fluorescence turn-ON linker for proteomic studies, Chem Commun 53 (2017) 13332–13335.
[26] J.T. Offenloch, J. Willenbacher, P. Tzvetkova, C. Heiler, H. Mutlu, C. Barner-Kowollik, Degradable fluorescent single-chain nanoparticles based on metathesis polymers, Chem Commun 53 (2017) 775–778.
[27] S.H. Lee, E. Moroz, B. Castagner, J.C. Leroux, Activatable cell penetrating peptide-peptide nucleic acid conjugate via reduction of azobenzene PEG chains, J Am Chem Soc 136 (2014) 12868–12871.
[28] H. Lei, M. Mo, D. Kong, Y. He, P. Zheng, L. Wu, Research progress on reduction cleavage of azo bonds in biological systems, Sci Sin Chim 48 (2018), https://doi.org/10.1360/N032018-00142.
[29] A. Priyam, K. Shivhare, S. Yadav, A.K. Sharma, P. Kumar, Enhanced solubility and self-assembly of amphiphilic sulfasalazine-PEG-OMe (S-PEG) conjugate into core-shell nanostructures useful for colonic drug delivery, Colloid Surf A 547 (2018) 157–167.
[30] X. Zhang, M. Wu, J. Li, S. Lan, Y. Zeng, X. Liu, J. Liu, Light-enhanced hypoxia-response of conjugated polymer nanocarrier for successive synergistic photodynamic and chemo-therapy, ACS Appl Mater Interf 10 (2018) 21909–21919.
[31] A.D. Wong, A.L. Prinzen, E.R. Gillies, Poly(ester amide)s with pendant azobenzenes: multi-responsive self-immolative moieties for modulating polymer assemblies, Polym Chem 7 (2016) 1871–1881.
[32] T. Eom, W. Yoo, Y.-D. Lee, J.H. Park, Y. Choe, J. Bang, S. Kim, A. Khan, An activatable anticancer polymer–drug conjugate based on the self-immolative azobenzene motif, J Mater Chem B 5 (2017) 4574–4578.
[33] N. Shin, K. Hanaoka, W. Piao, T. Miyakawa, T. Fujisawa, S. Takeuchi, S. Takahashi, T. Komatsu, T. Ueno, T. Terai, T. Tahara, M. Tanokura, T. Nagano, Y. Urano, Development of an azoreductase-based reporter system with synthetic fluorogenic substrates, ACS Chem Biol 12 (2017) 558–563.
[34] J. Tang, C. Huang, J. Shu, J. Zheng, D. Ma, J. Li, R. Yang, Azoreductase and target simultaneously activated fluorescent monitoring for cytochrome c release under hypoxia, Anal Chem 90 (2018) 5865–5872.
[35] L. Zhang, Y. Wang, X. Zhang, X. Wei, X. Xiong, S. Zhou, Enzyme and redox dual-triggered intracellular release from actively targeted polymeric micelles, ACS Appl Mater Interf 9 (2017) 3388–3399.
[36] T. Eom, W. Yoo, S. Kim, A. Khan, Biologically activatable azobenzene polymers targeted at drug delivery and imaging applications, Biomaterials 185 (2018) 333–347.

[37] Lu. Zhengrong, Songqi Gao, Pavla Kopečková, Jindřich Kopeček, Synthesis of bioadhesive lectin-HPMA copolymer – cyclosporin conjugates, Bioconjug Chem 11 (2000) 3–7.
[38] J. Rao, C. Hottinger, A. Khan, Enzyme-triggered cascade reactions and assembly of abiotic block copolymers into micellar nanostructures, J Am Chem Soc 136 (2014) 5872–5875.
[39] J. Rao, A. Khan, Enzyme sensitive synthetic polymer micelles based on the azobenzene motif, J Am Chem Soc 135 (2013) 14056–14059.
[40] J. Rao, A. Khan, Enzymatic 'charging' of synthetic polymers, Poly Chem 6 (2015) 686–690.
[41] C. Zhang, N. Jiao, Copper-catalyzed aerobic oxidative dehydrogenative coupling of anilines leading to aromatic azo compounds using dioxygen as an oxidant, Angew Chem Int Ed 49 (2010) 6174–6477.
[42] M. Mari, A. Morales, A. Colell, C. Garcia-Ruiz, N. Kaplowitz, J.C. Fernandez-Checa, Mitochondrial glutathione: features, regulation and role in disease, Biochim Biophys Acta 2013 (1830) 3317–3328.
[43] Monica Argenziano, Chiara Lombardi, Benedetta Ferrara, Francesco Trotta, Fabrizio Caldera, Marco Blangetti, et al., Glutathione/pH-responsive nanosponges enhance strigolactone delivery to prostate cancer cells, Oncotarget 9 (2018) 35813–35829.
[44] A.G. Milbradt, M. Loweneck, S.S. Krupka, M. Reif, E.K. Sinner, L. Moroder, C. Renner, Photomodulation of conformational states. IV. Integrin-binding RGD-peptides with (4-aminomethyl)phenylazobenzoic acid as backbone constituent, Biopolymer 77 (2005) 304–313.
[45] E.M. Kosower, H. Kanety-Londner, Glutathione. XIII Mechanism of thiol-oxidation by diazene-dicarboxylic acid derivatives, J Am Chem Soc 98 (1976) 3001–3007.
[46] J.B. Opalinska, B. Machalinski, J. Ratajczak, M.Z. Ratajczak, A.M. Gewirtz, Multigene targeting with antisense oligodeoxynucleotides: an exploratory study using primary human leukemia cells, Clin Cancer Res 11 (2005) 4948–4954.
[47] H. Fan, G. Yan, Z. Zhao, X. Hu, W. Zhang, H. Liu, X. Fu, T. Fu, X.B. Zhang, W. Tan, A smart photosensitizer-manganese dioxide nanosystem for enhanced photodynamic therapy by reducing glutathione levels in cancer cells, Angew Chem Int Ed 55 (2016) 5477–5482.
[48] F. Zhang, Q. Ni, O. Jacobson, S. Cheng, A. Liao, Z. Wang, Z. He, G. Yu, J. Song, Y. Ma, G. Niu, L. Zhang, G. Zhu, X. Chen, Polymeric nanoparticles with a glutathione-sensitive heterodimeric multifunctional prodrug for *in vivo* drug monitoring and synergistic cancer therapy, Angew Chem Int Ed 57 (2018) 7066–7070.